

## Restructuring G-Protein-Coupled Receptor Activation

Martin Audet<sup>1</sup> and Michel Bouvier<sup>1,\*</sup>

<sup>1</sup>Department of Biochemistry, Institute for Research in Immunology and Cancer, Université de Montréal, Montréal, QC H3C 3J7, Canada

\*Correspondence: [michel.bouvier@umontreal.ca](mailto:michel.bouvier@umontreal.ca)

<http://dx.doi.org/10.1016/j.cell.2012.09.003>

G-protein-coupled receptors serve as key signal transduction conduits, linking extracellular inputs with diverse cellular responses. These receptors eluded structural characterization for decades following their identification. A landmark structure of rhodopsin provided a basis for structure-function studies and homology modeling, but advances in receptor biology suffered from a lack of receptor-specific structural insights. The recent explosion in GPCR structures confirms some features predicted by rhodopsin-based models, and more importantly, it reveals unexpected ligand-binding modes and critical aspects of the receptor activation process. The new structures also promise to foster studies testing emerging models for GPCR function such as receptor dimerization and ligand-biased signaling.

### Introduction

G-protein-coupled receptors are seven transmembrane domain (TM) proteins that are located in the plasma membrane and transduce signals through their interactions with both extracellular small-molecule ligands and intracellular G proteins to initiate signaling cascades that allow cells to respond to changes within their environment. With more than 800 members in the human

of the conformational changes leading to the activation of G-protein-dependent and -independent signaling, thus yielding the needed information to understand drug action and support rational design.

Although GPCRs have been known for more than 40 years, the first high-resolution structure, that of the visual receptor rhodopsin, wasn't solved until 2000 (Palczewski et al., 2000),

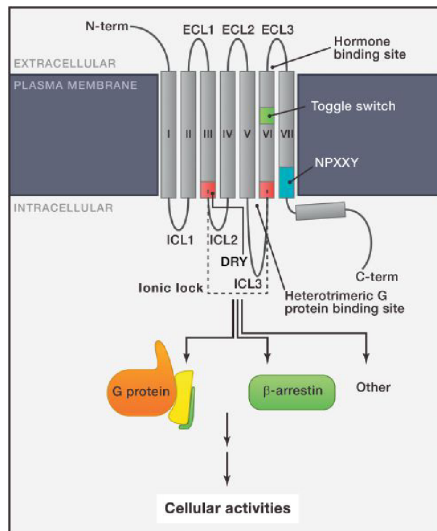


**Figure 1. G-Protein-Coupled Receptor Topological Organization and Signaling Paradigm**

Serpentine illustration of the seven transmembrane topological organization of GPCRs. The positions of some of the conserved structural features of the class A GPCRs such as the DRY and NPXXY motifs, as well as the toggle switch, are indicated. The dotted line indicates the two domains (in red) involved in the ionic interactions known as the ionic lock. The figure also illustrates the canonical G-protein-dependent and more recently described G-protein-independent signaling modes involving  $\beta$ -arrestin and other signaling effectors. ICL, intracellular loop; ECL, extracellular loop.

dark-adapted rhodopsin (Palczewski et al., 2000), which allowed an accurate determination of amino acid side chain conformations, as well as the extracellular and intracellular loops and the N- and C-terminal domains.

Collectively, the information gained from these models provided structural explanations for the role of specific sequence features that are highly conserved among the large class A subgroup of GPCRs that include rhodopsin, the monoamine receptors, and numerous peptide and lipid receptors. (This review will focus on class A receptors for which the principal structural advances have been realized.) It was previously shown for these receptors that a sequence element, termed the DRY (or E/DRY) motif, played a role in controlling receptor activity. The structural models revealed the presence of a polar interaction between an arginine located at the bottom of TMIII and a glutamate on TMVI, providing a structural explanation for the role of this conserved features. The so-called "ionic lock" formed between TMIII and TMVI was proposed to stabilize the inactive state of the receptor (Figures 1 and 2). Consistent with this notion, biophysical studies on rhodopsin (Altenbach et al., 2008) and the  $\beta_2$ -adrenergic receptor ( $\beta_2$ AR) (Yao et al., 2006)

**Table 1. GPCR Structures**

Receptor	Ligand	PDB Accession Number
<b>Inverse Agonists</b>		
Adenosine $A_{2A}$	caffeine	3RFM
	XAC	3REY
	ZM241385	3EML-3PWH-3VG9-3VGA
$\beta_2$ -adrenergic	carazolol	3KJ6-2RH1-2R4R-2R4S
	compound a <sup>a</sup>	3NY9
	ICI-118551	3NY8
	timolol	3D4S
Histamine $H_1$	doxepin	3RZE
$M_2$ muscarinic acetylcholine	QNB	3UON
$M_3$ muscarinic acetylcholine	tiotropium	4DAJ
<b>Antagonists</b>		
Adenosine $A_{2A}$	compound b <sup>b</sup>	3UZA
	compound c <sup>c</sup>	3UZC
$\beta_1$ -adrenergic	carazolol	2YCW
	cyanopindolol	2VT4-2YCX-2YCY
	iodocyanopindolol	2YCZ
$\beta_2$ -adrenergic	alprenolol	3NYA
CXC chemokine type 4	CVX15	3OE0
	IT1t	3ODU-3OE6-3OE8-3OE9
Dopamine D3	eticlopride	3PBL
$\delta$ opioid	naltrindol	4EJ4
$\kappa$ opioid	JD1c	4DJH
$\mu$ opioid	$\beta$ -funaltrexamine	4DKL
Nociceptin/orphanin FQ	G-24	4EA3
Sphingosine-1-phosphate type 1	ML056	3V2W
		3V2Y
<b>Agonists</b>		
$\beta_1$ -adrenergic	carmoterol	2Y02
	dobutamine	2Y00-2Y01
	isoproterenol	2Y03
	salbutamol	2Y04
$\beta_2$ -adrenergic	BI-167107	3P0G-3SN6
	procateterol	3PDS
Adenosine $A_{2A}$	adenosine	2YDO
	NECA	2YD0
	UK-432097	3QAK

Structures are grouped on the basis of the efficacy of the ligands that were cocrystallized: inverse agonists, antagonists, and agonists.

<sup>a</sup>Ethyl 4-[(2S)-2-hydroxy-3-[(propan-2-yl)amino]propoxy]-3-methyl-1-benzofuran-2-carboxylate.

<sup>b</sup>6-(2,6-dimethylpyridin-4-yl)-5-phenyl-1,2,4-triazin-3-amine.

<sup>c</sup>4-(3-amino-5-phenyl-1,2,4-triazin-6-yl)-2-chlorophenol.

showed that disruption of the interaction leads to TMVI movement away from the TM bundle, creating a crevice to cradle the heterotrimeric G protein. The similar findings for rhodopsin

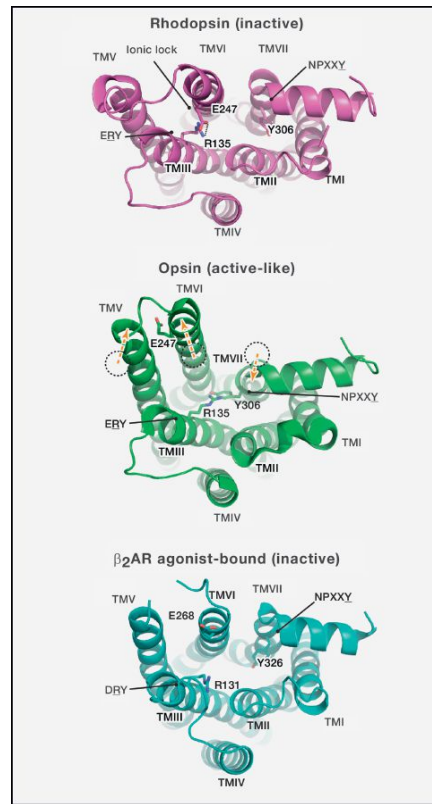


**Figure 2. Configurations of the "E/DRY," "Ionic Lock," and "NPXXY" Motifs in Rhodopsin, Opsin, and Antagonist-Bound  $\beta_2$ AR**

Bottom views of rhodopsin (PDB ID:1GZM), opsin (PDB ID:3DQB), and  $\beta_2$ -adrenergic receptor ( $\beta_2$ AR) (PDB ID:2RH1). TM domains are shown as ribbons, whereas the important residues of the E/DRY, ionic lock, and NPXXY motifs are shown as stick renderings and are indicated by solid lines. The structure of rhodopsin represents the inactive conformation of the receptor, whereas the opsin structure is in an active-like conformation. The dotted circles overlaid on the opsin structure indicate the positions of TMV, TMVI, and TMVII in the inactive rhodopsin, and the orange dotted arrows illustrate the TM movements from inactive to active states. The ionic interaction (ionic lock), represented by a dotted line between the R of the E/DRY motif and a negatively charged glutamate (E) residue in TMVI, is believed to stabilize the receptor in an inactive state. In the opsin structure, an active-like retinal-free state of rhodopsin, the disruption of the ionic lock allows TMVI to move away from the receptor bundle and down toward the cytoplasmic interface with the heterotrimeric G protein. Simultaneously, the tyrosine (Y) residue of the NPXXY motif moves inside the bundle, blocking TMVI in an open conformation. The ionic lock is, however, not found in most of the antagonist-bound GPCR structures obtained to date. This is exemplified here by the structure of the  $\beta_2$ AR bound to the antagonist (inverse agonist) carazolol, where the ionic lock is not formed, indicating that an alternative configuration is involved in the stabilization of the closed state of the receptor.

and the  $\beta_2$ AR popularized the notion that ligand binding would lead to full receptor activation through a common conserved mechanism. Yet, the lack of a 3D structure for an activated receptor prevented a complete understanding of the molecular processes linking ligand binding to receptor activation.

#### Methodological Breakthroughs

Seven years following the crystallization of mammalian rhodopsin, the structure of human  $\beta_2$ AR in complex with the  $\beta$ -adrenergic antagonist carazolol was solved (Cherezov et al., 2007; Rasmussen et al., 2007; Rosenbaum et al., 2007). Attaining this goal required major methodological hurdles to be overcome. First, large quantities of homogeneous receptor were needed—a task that was complicated by the lower expression of GPCRs binding diffusible ligands compared to rhodopsin. This problem was circumvented by overexpressing the receptors in specialized systems while the sources of microheterogeneity such as putative phosphorylation and glycosylation sites were eliminated by mutagenesis. Second, the stability of these intrinsically dynamic GPCRs needed to be increased to avoid aggregation and to facilitate crystal lattice packing. Because the third intracellular loop (ICL3) (Figure 1) is a particularly flexible domain, different strategies were designed to stabilize this part of the receptor. In a few cases (Rasmussen et al., 2007; Bokoch et al., 2010), an antibody Fab fragment recognizing ICL3 was bound to the receptor. In many other cases, ICL3 was deleted and replaced by well-folded soluble proteins such as T4 lysozyme (Chien et al., 2010; Jaakola et al., 2008; Rosenbaum et al., 2007; Wu et al., 2010, 2012) or the apocytochrome b564RIL (Thompson et al., 2012). Thermo-stabilizing mutations have also been used to obtain receptor preparations compatible with crystal formation (Warne et al., 2008; Doré et al., 2011; Lebon et al., 2011). The residues selected to stabilize the receptors were first identified empirically by testing a very large number of mutations and selecting those with the greatest impact on stability. In most cases, between four and eight mutations were needed to obtain the required stability.

As for many membrane proteins, GPCR crystallization requires conditions adapted to the hydrophobic nature of the protein. In an effort to satisfy this requirement, several methods, including detergent-based micelles, bicelles (Faham and Bowie, 2002), and in particular, lipidic cubic phase systems (Landau and Rosenbusch, 1996; Pebay-Peyroula et al., 1997), were developed and used successfully. Despite optimized conditions, GPCR crystals tend to be small. The development of microfocus X-ray synchrotron technologies that deliver a microscale beam to a crystal (Riek et al., 2005) greatly contributed to generating the high-resolution structures.

#### An Explosion of Structures

The wealth of structural information emerging over the last 5 years (Table 1) forms the basis of a real revolution in GPCR research. The structural and functional models that arise from them have changed our views on GPCR agonist and antagonist binding modes and on the activation processes.

#### Ligand Recognition

As expected, the overall folding of the TM domain is highly conserved among all structures and was well predicted by the

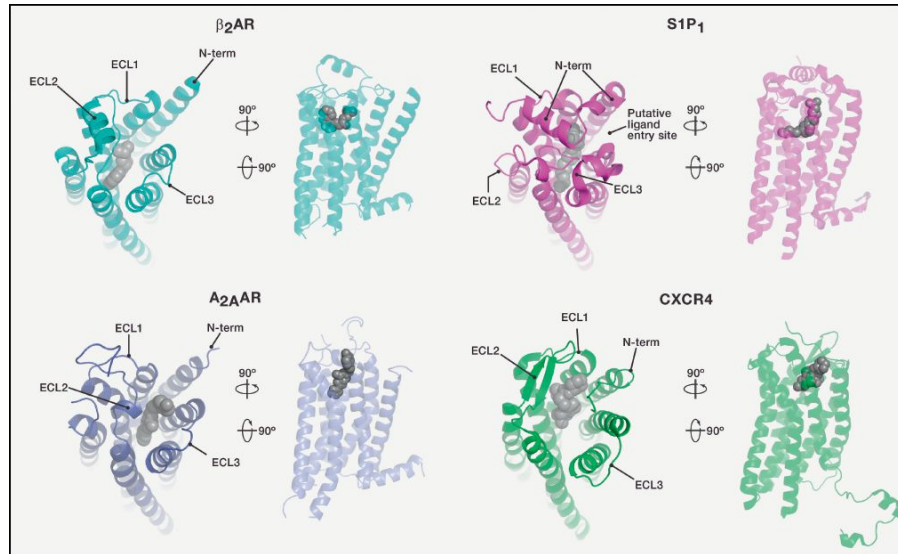


**Figure 3. Distinct Binding Modes for GPCR Ligands**

Top and side views of the human  $\beta_2$ AR (PDB ID:2RH1), S1P<sub>1</sub>R (PDB ID:3V2Y), human A<sub>2A</sub>AR (PDB ID:3EML), and human CXCR4 (PDB ID:3ODU) shown as ribbons with their respective cocrystallized ligand shown in gray spheres. The black solid lines indicate the position of the ECL and N terminus. The four receptors display different relative ligand orientations in the binding pocket and changes in the extracellular domain fold, revealing a great diversity in ligand binding. Interestingly,  $\beta_2$ AR, A<sub>2A</sub>AR, and CXCR4 have freely accessible binding pockets that are the consequence of a compact extracellular domain that does not obstruct the entry of ligands from the extracellular side. In contrast, the N terminus and ECL2 of S1P<sub>1</sub> extend on the top of the receptor, covering the opening of the receptor, thereby precluding any ligand exchange with the extracellular compartment. Therefore, an alternative path for ligand entry has been proposed between TM1 and TMVII.

structures of eukaryotic rhodopsin, showing only modest differences in the relative orientation of the TMs. However, more striking differences are found in the extracellular loop domains and especially in the second extracellular loop (ECL2) that clearly displays receptor-specific folds (Figure 3). These domains act as a vestibule directing the way ligands access the receptor-binding pocket. For example, the ECL2 of many receptors, including the  $\beta_2$ AR (Figure 3, top left), form a compact helical shape adjacent to the TM bundle that, along with the small ECL1 and ECL3, allows soluble ligands to diffuse easily from the extracellular compartment toward the binding site inside of the receptor bundle (Rosenbaum et al., 2007). In contrast, as was observed for rhodopsin (albeit through a different fold), the ECL2 of the S1P<sub>1</sub> receptor, along with ECL1 and the N-terminal helices, seals off the ligand-binding pocket (Figure 3, top right), blocking access from the extracellular milieu (Hanson et al., 2012). The structure suggests that the lipid agonist S1P accesses the receptor by a TMI-TMVII intrabundle opening near the plasma membrane. Interestingly, the extent of opening of each receptor's "mouth" determined by the relative position of ECL2 varies considerably between receptors, revealing an unex-

pected diversity of ligand entry mechanisms. In addition to their role in channeling the ligands toward the binding pocket, these extracellular domains have been suggested to contribute to both binding kinetics and selectivity (Dror et al., 2011).

As the structures have revealed diversity in how ligands access the receptor, so too have they illuminated specific aspects of ligand recognition. Classical views of how ligands might bind were sculpted by generalization from the retinal/rhodopsin structure (Palczewski et al., 2000) and early aminergic receptor modeling (Flower, 1999), in which ligands were predicted to lie parallel to the plane of the membrane deep in the TM bundle (Figure 3, top left). The new structures broaden our understanding on this front. For instance, both agonists and antagonists (Figure 3, bottom left) of A<sub>2A</sub> adenosine receptor (A<sub>2A</sub>AR) bind in an extended conformation perpendicular to the plane of the membrane where they are stabilized by extensive contacts with ECL2 and ECL3 (Doré et al., 2011; Jaakola et al., 2008; Xu et al., 2011). For CXCR4 (Figure 3, bottom right), the antagonist IT1t unexpectedly binds the receptor at its surface between TMVII, TMI, TMII, and ECL2 (Wu et al., 2010). In contrast,  $\beta_2$ AR shows the "canonical" deep TMVI-TMIII-TMV

aminergic binding pocket (Figure 3, top left), as do the muscarinic M2 and M3 receptors (M2R and M3R), although ligands for these latter receptors are protected by a three-dimensional aromatic cage (Haga et al., 2012; Kruse et al., 2012). Similarly, the S1P<sub>1</sub>R antagonist ML056 (Figure 3, top right) binds a highly hydrophobic and polyaromatic region deep in the receptor, but the ligand also projects phosphate and amine groups vertically toward charged and polar residues packed between the N-termini, ECL2, TMVII, TMII, and TMIII (Hanson et al., 2012). It should also be noted that the size of the binding sites greatly diverges among receptors, ranging from the small compact binding pocket of the eticlopride-bound dopamine receptor (Chien et al., 2010) to the large surface of the CXCR4-binding pocket required to accommodate the fold of the bound CVX15 peptide (Wu et al., 2010). These results clearly indicate that each receptor has a binding site that is specifically adapted to the nature of its ligands. These data open new perspective in the rational design of ligands that are better adapted to unique binding pockets.

The rich diversity of the ligand-receptor complexes indicates that ligand selectivity cannot be simply explained by different amino acids within shared ligand binding pockets, but that it also depends on the overall receptor architecture involving residues in different domains of the receptor. A good example is provided by the  $\beta_1$ AR and  $\beta_2$ AR structures that revealed a very high degree of identity between the residues found in the “canonical” aminergic binding pocket (Warne et al., 2008) despite the existence of clear receptor subtype selectivity. Such selectivity has been proposed to result in part from ligand-induced conformational changes (Wacker et al., 2010) and to involve interactions with ECL residues (Audet and Bouvier, 2008; Rosenbaum et al., 2007; Warne et al., 2008). A role for residues close to the extracellular domains in determining the ligand binding selectivity was also observed for the recently solved structure of the delta-opioid receptor (Granier et al., 2012). The crystal structure of the nociceptive/orphanin FQ receptor (NOP) also shows that most of the residues that are different between NOP and the other members of the opioid receptor family are not in direct contact with the ligand in the binding pocket but rather are involved in large pocket reshaping and water coordination.

The diversity in binding modes also has important implications for the activation process of the receptors, as it suggests that no unique activation trigger can be invoked for all GPCRs. Instead, the engagement of distinct regions of the receptors by their ligands predicts that different allosteric transitions will be needed to reach a common active state.

#### **Activation and Allosteric Transition**

GPCR ligands can be divided into two general classes: agonists that promote and antagonists that block receptor activation. Antagonists can be subdivided into inverse agonists, which inhibit the spontaneous (agonist-independent) activity of the receptors, and neutral antagonists that are devoid of intrinsic activity and block the action of both agonists and inverse agonists. Out of the 47 ligand-bound GPCR structures, 36 were cocrystallized with antagonists (including 16 with inverse agonists), whereas 11 were cocrystallized with agonists (Table 1). Somewhat surprisingly, few differences could be seen

between the agonist and antagonist-bound forms, yielding relatively little information on the dynamics of receptor activation and on the conformational changes underlying ligand-promoted activation. Exemplifying this point is the observation that structures of the G-protein-free  $\beta_2$ AR cocrystallized with full or partial agonists are very similar to those with antagonist or inverse agonist and mostly display the characteristics of an inactive conformation (Figure 4). These limited changes are consistent with a model for full GPCR activation that requires both ligand binding and G protein engagement.

Fortunately, three structures provided significant insights in the activation mechanism. The first one is a ligand-free form of opsin that is cocrystallized with the C terminus of the  $\alpha$ -subunit of the heterotrimeric visual G protein, transducin (Scheerer et al., 2008). This structure confirmed earlier predictions about TMVI movement from site-directed mutagenesis and biophysical studies. When compared with dark-adapted rhodopsin, a large outward movement of TMVI and disruption of the ionic lock between TMIII and TMVI were observed (Figure 2). In addition, this structure provided new insight into conformational rearrangements that facilitate G protein binding. In the active opsin, TMVII bends inward, allowing the repositioning of the tyrosine from the conserved NPXXY motif, which prevents the reverse movement of TMVI, thus stabilizing the open state that forms a cradle for transducin (Figure 2). In parallel, the arginine of the DRY motif juts into the bundle of the receptor, providing an interacting floor for transducin's C terminus. TMV is also repacked against TMVI, offering an additional interacting surface for the G protein.

The two additional structures that provided insights into the activation process are the agonist-bound  $\beta_2$ AR stabilized in the active conformation by a nanobody mimicking the G protein (Rasmussen et al., 2011a) and the agonist-bound  $\beta_2$ AR cocrystallized with heterotrimeric stimulatory G protein (G $\alpha$ s $\beta$ 1 $\gamma$ 2) (Rasmussen et al., 2011b). The C terminus of G $\alpha$ s lies deep in a pocket created by the outward movement of TMVI, and most of the G $\alpha$  interaction sites are found on TMIII, TMV, TMVI, and ICL2 of the receptor. As shown in Figure 4B, comparison of the agonist-bound G-protein-coupled  $\beta_2$ AR structure with that of the G-protein-free receptor bound to the inverse agonist carazolol showed significant conformational rearrangements that are similar to those observed for the active opsin. The noticeable differences were a larger outward movement and bending of TMVI and the formation of a bulge in TMV that positions a serine residue (S207) closer to the agonist, providing a structural explanation for the well-known increase in agonist affinity promoted by G protein coupling. Together, these changes represent key determinants of the allosteric transition toward a receptor state activating the G protein.

#### **Nucleotide Exchange**

The three structures that incorporate fragments of G proteins or G-protein-mimetics also provide insight into how GPCRs facilitate nucleotide exchange and, hence, initiate signaling cascades. The receptor-coupled structures of the G proteins show that the helical domain of G $\alpha$  undergoes a major rigid-body rotation of almost 130° upon receptor engagement (Figure 4B) that was previously predicted by modeling (Cherfils and Chabre, 2003) and biophysical studies (Galés et al., 2006).

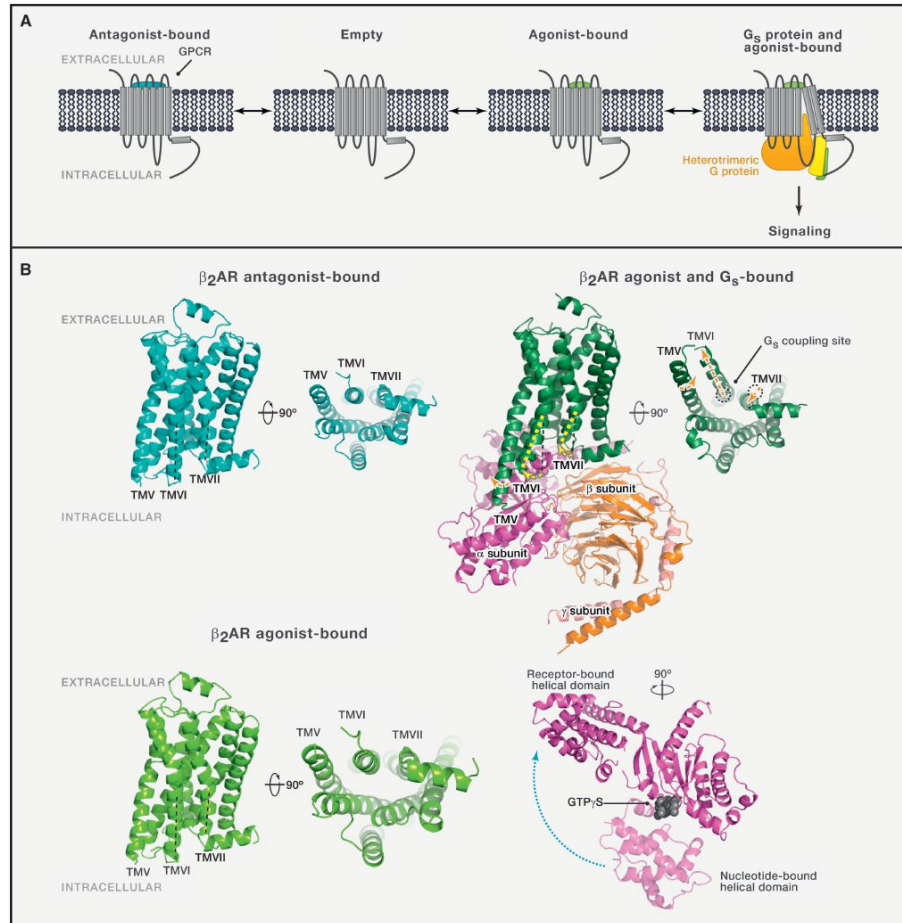


**Figure 4. Fully Activated Conformations Require the Presence of Both Agonist and G Protein**

(A) Schematic illustration of ligand binding and G protein engagement leading to a fully activated conformation of a receptor. (B) Side and bottom views of the  $\beta_2$ AR. Top left, bound to the antagonist (inverse agonist) carazolol (PDB ID: 2RH1); bottom left, covalently bound to the agonist procaterol (PDB ID: 3PDS); and top right, bound to the agonist BI-167107 in the presence of  $G_{\alpha_s} \beta_1 \gamma_2$  (PDB ID: 3SN6). Black dotted lines and circles illustrate the position of TMVI and TMVII in the inverse agonist-bound (inactive state) structure, whereas yellow dotted lines illustrate their position in the  $G_s$  and agonist-bound structure (active state). The TM movements from the inactive to active states are indicated by yellow and orange arrows. It should be noted that the large movements of the receptor leading to its open and active conformation were observed only in the presence of both agonist and G protein (top right). The structure obtained in the presence of the agonist alone (bottom left) was similar to the inactive structure obtained in the presence of inverse agonist (top left). To illustrate the conformational rearrangement of the G protein during the activation process, the helical domain structure of the nucleotide (GTP $\gamma$ S)-bound heterotrimeric  $G_s$  (PDB ID: 1AZS) was overlaid on the structure of the receptor-bound  $G_s$  (bottom right). The blue dotted arrow indicates the large rigid-body movement of the helical domain of  $G_{\alpha_s}$  that suggests a possible structural basis for the nucleotide exchange promoted by receptor activation.

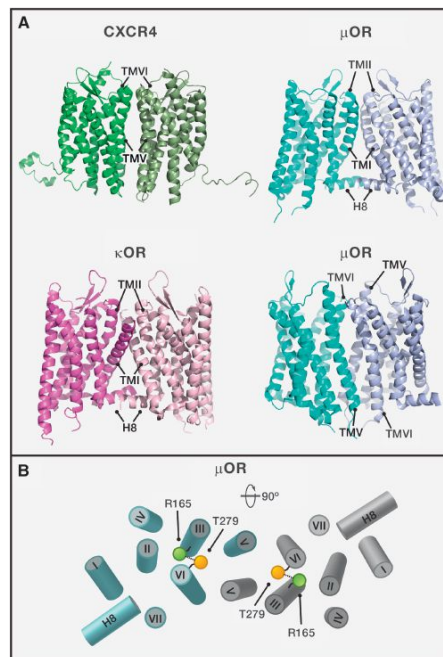


**Figure 5. Possible Dimerization Interfaces Revealed by GPCR Crystal Structures**

(A) Side views of CXCR4 (PDB ID: 3ODU), μOR (PDB ID: 4DKL), and κOR (PDB ID: 4DJH) dimers. The position of the TM domains at the dimerization interface is indicated by solid black lines. Both TMI-TMI-helix 8 (H8) and TMV-TMVI interfaces are found in the μOR, suggesting a plausible structural basis for the formation of higher-order oligomers.

(B) Schematic illustration of a possible mechanism for interprotomer allosteric regulation of receptor activity involving R165 of the DRY motif and a threonine residue (T279) that lies at the TMV-TMVI interface of the μOR dimer. Interactions between R165 and T279 are shown by a dotted line.

observation that T279, which stabilizes the closed position of TMVI in the inactive receptor state by interacting with R165 of the DRY motif, is packed within the TMV-TMVI interface offers a possible mechanism for interprotomer regulation of receptor activity (Figure 5). However, the TM5-TM6 interface is not present in the κ-opioid receptor (κOR) dimer structure. Indeed, only one interface (1100 Å<sup>2</sup> of buried surface), involving the TMI, TMII, and helix 8, is visible in this structure (Wu et al., 2012). The absence of the TMV-TMVI interface in the κOR structure is somewhat surprising given the high level of sequence identity with the μOR in these TMs and may be due to the steric hindrance from the two T4 lysozyme inserts included to aid crystallization of κOR. Whether the dimerization interfaces revealed by the recently solved structures correspond to the functionally

relevant dimers will require additional studies involving site-directed mutagenesis and biochemical and biophysical approaches, but the structures provide rational starting points for this work.

### Conclusion

The recent flurry of high-resolution GPCR structures represents a true renaissance for GPCR research. Although much remains to be done to fully understand the precise molecular mechanisms controlling receptor activities, the achievements of the last 5 years provide the foundation of what promises to be very exciting times for structure-based molecular pharmacology and drug discovery. An emerging theme stems from the observation that GPCRs function as molecular hubs that can engage several distinct G proteins, as well as G-protein-independent signaling pathways, and that different ligands promote the engagement of distinct subsets of effectors (Galandrin et al., 2007). At the molecular level, such ligand-biased signaling is believed to result from the stabilization of different active conformations of the receptors (Bokoch et al., 2010). A future challenge for structural biology will therefore be to provide high-resolution images of these different receptor states with the goal of designing ligands—and ultimately drugs—to selectively control specific functions. As discussed above, the structures obtained when cocrystallizing receptors with ligands displaying distinct efficacy profiles revealed very similar structures, indicating that solving the structures of receptor-ligand complexes may not be sufficient to fully explore the conformational plasticity of GPCRs underlying their rich biology. The observation that cocrystallization with a G protein or a mimic was needed to reveal a fully active conformation suggests that solving structures of GPCRs in complex with specific effectors such as different G proteins, β-arrestins, or GPCR kinases will be needed to unravel the true diversity of receptor conformations.

### ACKNOWLEDGMENTS

We thank Drs. Monique Lagacé and Marc Therrien for their critical reading of the manuscript. M.B. holds the Canada Research Chair in Signal Transduction and Molecular Pharmacology.

### REFERENCES

- Altenbach, C., Kusnetzow, A.K., Ernst, O.P., Hofmann, K.P., and Hubbell, W.L. (2008). High-resolution distance mapping in rhodopsin reveals the pattern of helix movement due to activation. *Proc. Natl. Acad. Sci. USA* 105, 7439–7444.
- Angers, S., Salahpour, A., and Bouvier, M. (2002). Dimerization: an emerging concept for G protein-coupled receptor ontogeny and function. *Annu. Rev. Pharmacol. Toxicol.* 42, 409–435.
- Audet, M., and Bouvier, M. (2008). Insights into signaling from the beta2-adrenergic receptor structure. *Nat. Chem. Biol.* 4, 397–403.
- Baldwin, J.M., Schertler, G.F., and Unger, V.M. (1997). An alpha-carbon template for the transmembrane helices in the rhodopsin family of G-protein-coupled receptors. *J. Mol. Biol.* 272, 144–164.
- Bokoch, M.P., Zou, Y., Rasmussen, S.G., Liu, C.W., Nygaard, R., Rosenbaum, D.M., Fung, J.J., Choi, H.J., Thian, F.S., Kobilka, T.S., et al. (2010). Ligand-specific regulation of the extracellular surface of a G-protein-coupled receptor. *Nature* 463, 108–112.

- Cherezov, V., Rosenbaum, D.M., Hanson, M.A., Rasmussen, S.G., Thian, F.S., Kobilka, T.S., Choi, H.J., Kuhn, P., Weis, W.I., Kobilka, B.K., and Stevens, R.C. (2007). High-resolution crystal structure of an engineered human beta2-adrenergic G protein-coupled receptor. *Science* 318, 1258–1265.
- Cherfils, J., and Chabre, M. (2003). Activation of G-protein  $\alpha$  subunits by receptors through  $\alpha$ - $\beta$  and  $\alpha$ - $\gamma$  interactions. *Trends Biochem. Sci.* 28, 13–17.
- Chien, E.Y., Liu, W., Zhao, Q., Katritch, V., Han, G.W., Hanson, M.A., Shi, L., Newman, A.H., Javitch, J.A., Cherezov, V., and Stevens, R.C. (2010). Structure of the human dopamine D3 receptor in complex with a D2/D3 selective antagonist. *Science* 330, 1091–1095.
- Chung, K.Y., Rasmussen, S.G., Liu, T., Li, S., DeVree, B.T., Chae, P.S., Calinski, D., Kobilka, B.K., Woods, V.L., Jr., and Sunahara, R.K. (2011). Conformational changes in the G protein Gs induced by the  $\beta_2$  adrenergic receptor. *Nature* 477, 611–615.
- Doré, A.S., Robertson, N., Errey, J.C., Ng, I., Hollenstein, K., Tehan, B., Hurrell, E., Bennett, K., Congreve, M., Magnani, F., et al. (2011). Structure of the adenosine A(2A) receptor in complex with ZM241385 and the xanthines XAC and caffeine. *Structure* 19, 1283–1293.
- Dror, R.O., Pan, A.C., Arlow, D.H., Borhani, D.W., Maragakis, P., Shan, Y., Xu, H., and Shaw, D.E. (2011). Pathway and mechanism of drug binding to G-protein-coupled receptors. *Proc. Natl. Acad. Sci. USA* 108, 13118–13123.
- Faham, S., and Bowie, J.U. (2002). Bicelle crystallization: a new method for crystallizing membrane proteins yields a monomeric bacteriorhodopsin structure. *J. Mol. Biol.* 316, 1–6.
- Flower, D.R. (1999). Modelling G-protein-coupled receptors for drug design. *Biochim. Biophys. Acta* 1422, 207–234.
- Foord, S.M., Bonner, T.I., Neubig, R.R., Rosser, E.M., Pin, J.P., Davenport, A.P., Spedding, M., and Harmar, A.J. (2005). International Union of Pharmacology. XLVI. G protein-coupled receptor list. *Pharmacol. Rev.* 57, 279–288.
- Galandrin, S., Oligny-Longpré, G., and Bouvier, M. (2007). The evasive nature of drug efficacy: implications for drug discovery. *Trends Pharmacol. Sci.* 28, 423–430.
- Galés, C., Van Durm, J.J., Schaack, S., Pontier, S., Percherancier, Y., Audet, M., Paris, H., and Bouvier, M. (2006). Probing the activation-promoted structural rearrangements in preassembled receptor-G protein complexes. *Nat. Struct. Mol. Biol.* 13, 778–786.
- Granier, S., Manglik, A., Kruse, A.C., Kobilka, T.S., Thian, F.S., Weis, W.I., and Kobilka, B.K. (2012). Structure of the  $\delta$ -opioid receptor bound to naltrindole. *Nature* 485, 400–404.
- Haga, K., Kruse, A.C., Asada, H., Yurugi-Kobayashi, T., Shiroishi, M., Zhang, C., Weis, W.I., Okada, T., Kobilka, B.K., Haga, T., and Kobayashi, T. (2012). Structure of the human M2 muscarinic acetylcholine receptor bound to an antagonist. *Nature* 482, 547–551.
- Hanson, M.A., Roth, C.B., Jo, E., Griffith, M.T., Scott, F.L., Reinhart, G., Desale, H., Clemons, B., Cahalan, S.M., Schuerer, S.C., et al. (2012). Crystal structure of a lipid G protein-coupled receptor. *Science* 335, 851–855.
- Henderson, R., and Unwin, P.N.T. (1975). Three-dimensional model of purple membrane obtained by electron microscopy. *Nature* 257, 28–32.
- Henderson, R., Baldwin, J.M., Ceska, T.A., Zemlin, F., Beckmann, E., and Downing, K.H. (1990). Model for the structure of bacteriorhodopsin based on high-resolution electron cryo-microscopy. *J. Mol. Biol.* 213, 899–929.
- Jaakola, V.P., Griffith, M.T., Hanson, M.A., Cherezov, V., Chien, E.Y., Lane, J.R., Ijzerman, A.P., and Stevens, R.C. (2008). The 2.6 angstrom crystal structure of a human A2A adenosine receptor bound to an antagonist. *Science* 322, 1211–1217.
- Kruse, A.C., Hu, J., Pan, A.C., Arlow, D.H., Rosenbaum, D.M., Rosemond, E., Green, H.F., Liu, T., Chae, P.S., Dror, R.O., et al. (2012). Structure and dynamics of the M3 muscarinic acetylcholine receptor. *Nature* 482, 552–556.
- Landau, E.M., and Rosenbusch, J.P. (1996). Lipidic cubic phases: a novel concept for the crystallization of membrane proteins. *Proc. Natl. Acad. Sci. USA* 93, 14532–14535.
- Lebon, G., Warne, T., Edwards, P.C., Bennett, K., Langmead, C.J., Leslie, A.G., and Tate, C.G. (2011). Agonist-bound adenosine A2A receptor structures reveal common features of GPCR activation. *Nature* 474, 521–525.
- Manglik, A., Kruse, A.C., Kobilka, T.S., Thian, F.S., Mathiesen, J.M., Sunahara, R.K., Pardo, L., Weis, W.I., Kobilka, B.K., and Granier, S. (2012). Crystal structure of the  $\mu$ -opioid receptor bound to a morphinan antagonist. *Nature* 485, 321–326.
- Moukhametzanov, R., Warne, T., Edwards, P.C., Serrano-Vega, M.J., Leslie, A.G., Tate, C.G., and Schertler, G.F. (2011). Two distinct conformations of helix 6 observed in antagonist-bound structures of a beta1-adrenergic receptor. *Proc. Natl. Acad. Sci. USA* 108, 8228–8232.
- Palczewski, K., Kumasaka, T., Hori, T., Behnke, C.A., Motoshima, H., Fox, B.A., Le Trong, I., Teller, D.C., Okada, T., Stenkamp, R.E., et al. (2000). Crystal structure of rhodopsin: A G protein-coupled receptor. *Science* 289, 739–745.
- Pebay-Peyroula, E., Rummel, G., Rosenbusch, J.P., and Landau, E.M. (1997). X-ray structure of bacteriorhodopsin at 2.5 angstroms from microcrystals grown in lipidic cubic phases. *Science* 277, 1676–1681.
- Rasmussen, S.G., Choi, H.J., Rosenbaum, D.M., Kobilka, T.S., Thian, F.S., Edwards, P.C., Burghammer, M., Ratnala, V.R., Sarishvili, R., Fischetti, R.F., et al. (2007). Crystal structure of the human beta2 adrenergic G-protein-coupled receptor. *Nature* 450, 383–387.
- Rasmussen, S.G., Choi, H.J., Fung, J.J., Pardon, E., Casarosa, P., Chae, P.S., DeVree, B.T., Rosenbaum, D.M., Thian, F.S., Kobilka, T.S., et al. (2011a). Structure of a nanobody-stabilized active state of the  $\beta_2$  adrenoceptor. *Nature* 469, 175–180.
- Rasmussen, S.G., DeVree, B.T., Zou, Y., Kruse, A.C., Chung, K.Y., Kobilka, T.S., Thian, F.S., Chae, P.S., Pardon, E., Calinski, D., et al. (2011b). Crystal structure of the  $\beta_2$  adrenergic receptor-Gs protein complex. *Nature* 477, 549–555.
- Riek, C., Burghammer, M., and Schertler, G. (2005). Protein crystallography microdiffraction. *Curr. Opin. Struct. Biol.* 15, 556–562.
- Rosenbaum, D.M., Cherezov, V., Hanson, M.A., Rasmussen, S.G., Thian, F.S., Kobilka, T.S., Choi, H.J., Yao, X.J., Weis, W.I., Stevens, R.C., and Kobilka, B.K. (2007). GPCR engineering yields high-resolution structural insights into beta2-adrenergic receptor function. *Science* 318, 1266–1273.
- Scheerer, P., Park, J.H., Hildebrand, P.W., Kim, Y.J., Krauss, N., Choe, H.W., Hofmann, K.P., and Ernst, O.P. (2008). Crystal structure of opsin in its G-protein-interacting conformation. *Nature* 455, 497–502.
- Schertler, G.F.X., Villa, C., and Henderson, R. (1993). Projection structure of rhodopsin. *Nature* 362, 770–772.
- Thompson, A.A., Liu, W., Chun, E., Katritch, V., Wu, H., Vardy, E., Huang, X.P., Trapella, C., Guerrini, R., Calo, G., et al. (2012). Structure of the nociceptin/orphanin FQ receptor in complex with a peptide mimetic. *Nature* 485, 395–399.
- Wacker, D., Fenalti, G., Brown, M.A., Katritch, V., Abagyan, R., Cherezov, V., and Stevens, R.C. (2010). Conserved binding mode of human beta2 adrenergic receptor inverse agonists and antagonist revealed by X-ray crystallography. *J. Am. Chem. Soc.* 132, 11443–11445.
- Wall, M.A., Coleman, D.E., Lee, E., Iñiguez-Lluhi, J.A., Posner, B.A., Gilman, A.G., and Sprang, S.R. (1995). The structure of the G protein heterotrimer G $\alpha_1\beta_1\gamma_2$ . *Cell* 83, 1047–1058.
- Warne, T., Serrano-Vega, M.J., Baker, J.G., Moukhametzanov, R., Edwards, P.C., Henderson, R., Leslie, A.G., Tate, C.G., and Schertler, G.F. (2008). Structure of a beta1-adrenergic G-protein-coupled receptor. *Nature* 454, 486–491.
- Warne, T., Moukhametzanov, R., Baker, J.G., Nehmé, R., Edwards, P.C., Leslie, A.G., Schertler, G.F., and Tate, C.G. (2011). The structural basis for agonist and partial agonist action on a  $\beta_1$ -adrenergic receptor. *Nature* 469, 241–244.